Inter-pigment interactions in the peridinin chlorophyll protein studied by global and target analysis of time resolved absorption spectra. Chem Phys

ARTICLE *in* CHEMICAL PHYSICS · FEBRUARY 2009

Impact Factor: 1.65 · DOI: 10.1016/j.chemphys.2008.10.005

Chemical Physics 357 (2009) 70–78

Contents lists available at ScienceDirect

Chemical Physics

journal homepage: www.elsevier.com/locate/chemphys

Inter-pigment interactions in the peridinin chlorophyll protein studied by global and target analysis of time resolved absorption spectra

Ivo H.M. van Stokkum [a,*], Emmanouil Papagiannakis [a], Mikas Vengris [a,1], Jante M. Salverda [a,2], Tomáš Polívka [b,3], Donatas Zigmantas [b], Delmar S. Larsen [a,4], Stefania S. Lampoura [a,5], Roger G. Hiller [c], Rienk van Grondelle [a]

[a] Department of Physics and Astronomy, Faculty of Sciences, VU University Amsterdam, De Boelelaan 1081, 1081 HV Amsterdam, The Netherlands
[b] Department of Chemical Physics, Lund University, Lund, Sweden
[c] School of Biological Sciences, Macquarie University, NSW 2109, Australia

ARTICLE INFO

Article history:
Received 3 June 2008
Accepted 2 October 2008
Available online 15 October 2008

Keywords:
Peridinin chlorophyll protein
Global analysis
Target analysis
Time resolved absorption spectroscopy

ABSTRACT

Inter-pigment interactions define the functioning of light-harvesting protein complexes. To describe the particularly complex molecular dynamics and interactions of peridinin and chlorophyll in the peridinin chlorophyll protein of *Amphidinium carterae*, we applied global and target analysis to a series of ultrafast transient absorption experiments. We have created and validated a model that consistently describes and characterizes the interactions and evolution of excited and ground-state populations after excitation in all different experiments. The series of energy transfer steps that follow excitation are described by our model of cascading populations and numerous rate constants that correspond to intra-molecular thermal relaxation, fast and slow peridinin-to-chlorophyll energy transfer steps, and chlorophyll excited-state annihilation. By analyzing the spectral response of ground-state peridinins to excited chlorophylls we have identified which specific peridinin molecule is most closely coupled to the chlorophylls. No evidence was found that the intra-molecular charge transfer (ICT) state of peridinin, identified in studies of peridinin in solution, is a separate entity in the protein. The peridinin that exhibited slow peridinin-to-chlorophyll energy transfer was characterized by a difference spectrum free from ICT features, consistent with the importance of coupled ICT and S_1 states for energy transfer.

1. Introduction

Dinoflagellates, oceanic photosynthetic algae, contain light-harvesting complexes with enhanced absorption of blue–green light that feed excitation into the membrane-associated photosynthetic apparatus. These light-harvesting complexes contain a relatively large amount of carotenoids, which color the organism red, brown or orange [1]. The peridinin chlorophyll protein (PCP) of *Amphidinium carterae* [2], whose crystal structure has been resolved to a 2 Å resolution [3], is such a complex, as recently reviewed in [4]. PCP is water soluble rather than membrane bound as are most light-harvesting complexes and *in vivo* forms a trimeric complex that attaches itself to the photosystem II supercomplex to transfer energy to the photosystem II reaction center.

A large number of theoretical and experimental studies have focused on PCP [5–19], which is an ideal system to study pigment–pigment interactions for a variety of reasons; its structure is known, it has the highest observed relative carotenoid content, binding peridinin and chlorophyll-*a* (Chl-*a*) molecules in a 4:1 ratio, and furthermore, it binds peridinin which is a carotenoid that exhibits unique spectroscopic properties [9,14,20–26]. The organization of the pigments in the monomeric unit of PCP is shown in Fig. 1. The pigments are arranged in two quasi-symmetric clusters which are contained in a single hydrophobic cavity of the protein and comprise one chlorophyll and four peridinin molecules each. Each of the chlorophylls is very close to its associated peridinins, with an edge-to-edge distance of ≈5 Å to all four of them. In

Abbreviations: Chl, chlorophyll; DADS, decay associated difference spectrum; EADS, evolution associated difference spectrum; EET, excitation energy transfer; ESA, excited-state absorption; FWHM, full width at half maximum; ICT, intra-molecular charge transfer; IRF, instrument response function; MA, magic angle; PCP, peridinin-chlorophyll protein; Per, peridinin; SAS,species associated spectrum; SADS, species associated difference spectrum; SE, stimulated emission.

* Corresponding author. Tel.: +31 20 5987868; fax: +31 20 5987999.
E-mail address: ivo@nat.vu.nl (I.H.M. van Stokkum).

[1] Present address: Laser Research Centre, Faculty of Physics, Vilnius University, Vilnius, Lithuania.
[2] Present address: Biophysics, Leiden Institute of Physics, Leiden University, Leiden, The Netherlands.
[3] Present address: Institute of Physical Biology, University of South Bohemia, Nove Hrady, Czech Republic.
[4] Present address: Department of Chemistry, University of California, Davis, California, USA.
[5] Present address: Aen Makedonias, Michaniona, Thessaloniki, Greece.

0301-0104/$ - see front matter © 2008 Elsevier B.V. All rights reserved.
doi:10.1016/j.chemphys.2008.10.005

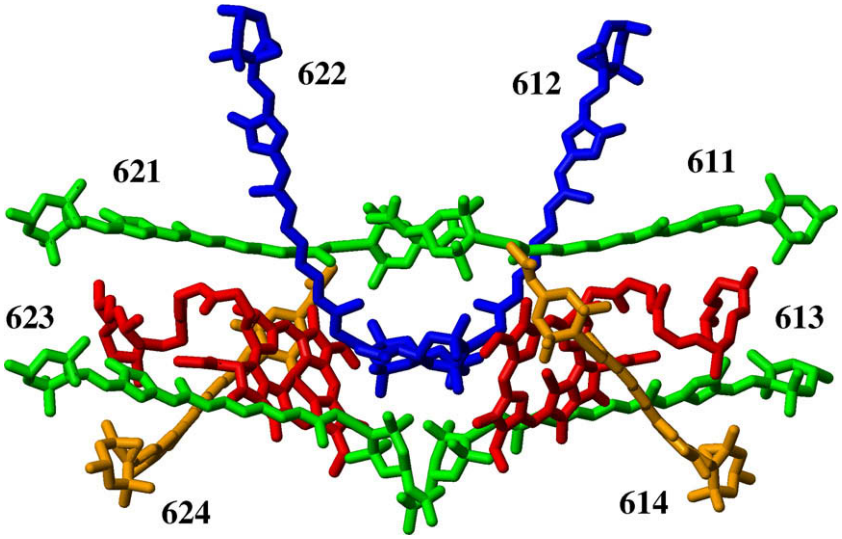

Fig. 1. Arrangement of pigments in PCP monomer. Key: peridinin (blue, green, orange), Chl-a (red). Numbers refer to the peridinin notation based on PDB entry 1PPR [3]. (For interpretation of color in this figure, the reader is referred to the web version of this article.)

contrast, the two chlorophyll molecules are not very close to each other at a distance of 17.4 Å [3].

The pigment composition and geometry in PCP is suggestive of their function; the absorption spectrum in Fig. 2 illustrates that peridinins are crucial light-harvesters, as the chlorophylls exhibit relatively weak features at 435 nm (Soret) and 670 nm (Q_y). The peridinin absorption band is intense and extends from 400 to 550 nm. This absorbance, as in all carotenoids, corresponds to the transition from the ground to the S_2 state by the absorption of one photon [27]. Studies on excitation energy transfer (EET) in PCP have shown that peridinin has an overall ≈90% efficiency of donating its singlet energy to chlorophylls [5,10]. Despite prediction from calculations that no EET proceeds from the S_2 state of peridinin [8], transient absorption experiments have demonstrated that ≈30% of the absorbed energy is transferred to chlorophylls directly from the S_2 state [6,7].

Studies of peridinin in various solvents have illustrated that, as a result of its functional groups, the singlet excited-state manifold is particularly complex; it includes an intra-molecular charge transfer (ICT) state which coexists with the "normal" S_1 state of typical carotenoids [20,21]. This ICT state, which is observed in polar (e.g. methanol) but not in non-polar solvents (e.g. hexane) is characterized by an excited-state absorption (ESA) that is red-shifted compared to that of pure S_1 as observed in hexane [20–23] and by a stimulated emission (SE) band that appears in the near infrared region [21,22]. The SE band of the ICT state was also observed in PCP, where, after the excitation of peridinin, its decay dynamics are correlated with the rise of the chlorophyll signal, leading to the conclusion that the ICT is a major energy funnel towards chlorophyll [7]. Pump-dump-probe experiments have shown that for peridinin dissolved in methanol the S_1 and the ICT states are separate entities, that equilibrate on the timescale of a few picoseconds [23,26]. In PCP, both the S_1 and ICT state are thought to participate in the EET process, which occurs on a picosecond timescale.

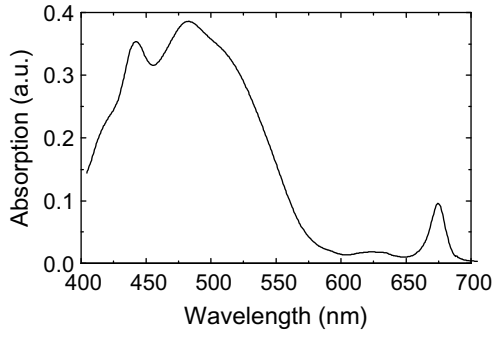

Fig. 2. Absorption spectrum of PCP.

The current study aims at characterizing the interactions between the peridinins and the chlorophylls in PCP by using ultrafast transient absorption techniques and global and target analysis methodologies. First we will address the interaction between excited peridinin molecules and the chlorophylls in PCP. We will then present a target analysis model that captures the essence of the peridinin-to-chlorophyll energy transfer processes in PCP and describes the spectral and temporal properties of the involved states. This model will also be tested with low temperature data. In the second part, we will present and discuss the results of a multi-pump transient absorption experiment, where a 500-nm pulse is used to excite peridinins while the chlorophylls in PCP have been pre-excited by a 400-nm pulse and are in their excited state. Finally, we directly excite the chlorophylls in PCP and address their interaction with the ground-state peridinins, which allows us to identify the interaction between the chlorophyll and a specific peridinin.

2. Materials and methods

2.1. Sample preparation

PCP complexes from *A. carterae*, isolated as described earlier [2], were dissolved in an aqueous buffer with 25 mM TRIS, 2 mM KCl and a pH of 7.5. At the concentrations used PCP will be mostly in its trimeric form.

2.2. Transient absorption spectroscopy

Ultrafast transient absorption measurements were performed with a set-up described in detail earlier [28,29]. The basis of the system is a 1-kHz amplified Ti:Sapphire system (Coherent-BMi α1000) delivering 450-μJ, 60-fs, 800-nm pulses. Part of the output of the amplifier was used to pump a homemade non-collinear optical parametric amplifier (NOPA) which generates visible pulses that can be tuned for selective pigment excitation. For the

multi-pump experiment [30], we used an additional 800-nm beam line; a BBO crystal was used to generate 400-nm pulses to excite the chlorophyll in the Soret region, while a delay line enabled the individual timing of these pulses. A small part of the 800-nm light was used for generating single-filament white light continuum in a slowly translating CaF_2 crystal for broad-band probing. Reflective optics have been used to steer and focus the white light probe beam to the sample, decreasing the group velocity dispersion to typically ≈300 fs over the range of 400–700 nm. After the spatial overlap of the pump and probe beams in the sample, the probe beam was dispersed by a spectrograph and projected on a home-built diode-array detector. The polarization of the pump pulses was set at magic angle (54.7°) compared to that of the probe light. For the anisotropy measurements [31], a Berek compensator in the path of the pump beam was used to adjust the polarization of the pump beam to parallel and perpendicular to that of the probe beam. For the measurements at 77 K [32] glycerol (2/1 v/v) was added for clear-glass formation at low temperatures, and samples were inserted into an Oxford cryostat.

2.3. Data analysis

The global and target analysis methods used here have been reviewed in [33,34]. Briefly, the basis of global analysis is the superposition principle, which states that the measured data $\psi(t,\lambda)$ result from a superposition of the spectral properties $\varepsilon_l(\lambda)$ of the components present in the system of interest weighted by their concentration $c_l(t)$.

$$\psi(t,\lambda) = \sum_{l=1}^{n_{\mathrm{comp}}} c_l(t)\varepsilon_l(\lambda)$$

The $c_l(t)$ of all n_{comp} components are described by a compartmental model, that consists of first-order differential equations, with as solution sums of exponential decays. We will consider three types of compartmental models: (1) a model with components decaying monoexponentially in parallel, which yields decay associated difference spectra (DADS), (2) a sequential model with increasing lifetimes, also called an unbranched unidirectional model, resulting in evolution associated difference spectra (EADS), and (3) a full compartmental scheme which may include possible branchings and equilibria, yielding species associated difference spectra (SADS). The latter is most often referred to as target analysis, where the target is the proposed kinetic scheme, including possible spectral assumptions. The instrument response function (IRF) can usually adequately be modeled with a Gaussian with parameters for location and full width at half maximum (FWHM, typically 100–250 fs). The dispersion of this location parameter is described by a polynomial. All exponential decays from the above models have to be convolved with the IRF.

When in addition to magic angle (MA) data also parallel (VV) and perpendicular (VH) data are collected, more information is available to disentangle the complex kinetics, and estimate the species associated spectra (SAS). In such an extended target analysis the magic angle concentrations c_l^{MA} are multiplied by the anisotropic properties of the components.

$$\begin{bmatrix} \mathrm{MA}(t,\lambda) \\ \mathrm{VV}(t,\lambda) \\ \mathrm{VH}(t,\lambda) \end{bmatrix} = \sum_{l=1}^{n_{\mathrm{comp}}} c_l^{\mathrm{MA}} \mathrm{SAS}_l(\lambda) \begin{bmatrix} 1 \\ 1+2r_l(t) \\ 1-r_l(t) \end{bmatrix}$$

Each $r_l(t)$ is described as

$$r_l(t) = (r_{l0} - r_{l\infty})\exp(-t/\tau) + r_{l\infty}$$

When an anisotropy decay is present, each isotropic exponential decay has to be multiplied by the associated anisotropy decay before the convolution with the IRF. Note that bleach and excited-state absorption contributions to the SADS can be resolved in these experiments provided that their anisotropy functions $r_l(t)$ differ.

3. Results and discussion

3.1. Per*–Chl interactions: light-harvesting by peridinin, and Chl–Chl annihilation

Magic angle pump probe data measured after 500 nm excitation are depicted in Fig. S1. Global analysis of these data yielded five lifetimes of ≈0.06 ps (black), 0.6 ps (red), 2.3 ps (blue), 33 ps (green), 1.9 ns (magenta). The estimated DADS and EADS are shown in Fig. 3[6]. Around 670 nm the Chl Q_y bleach and stimulated emission are visible, which henceforth will be abbreviated as Chl Q_y bleach. The spectrum directly after excitation is the black EADS, which consists mainly of Per* in the S_2 state, with a bleach below 500 nm, stimulated emission around 540 nm, and excited-state absorption (ESA) above 600 nm. It is unknown why the Chl Q_y region already shows a bleach (superimposed upon the broad S_2 ESA) here, maybe a small fraction of Chl is directly excited. To resolve this question high quality data with higher time resolution would be needed. After approximately 60 fs the first EADS is replaced by the second EADS (red), where the ESA now starts from 540 nm. In turn, the red EADS evolves in 0.6 ps to the blue EADS, where the ESA has shifted further to the blue, and the superimposed Chl Q_y bleach has clearly increased. The blue EADS evolves in 2.3 ps to the green EADS, with most, but not all, of the Per* features disappearing. When comparing the normalized green and magenta EADS, it is clear that some Per* is still contained in the green EADS, as evidenced by Per* ESA and bleach superimposed upon the relatively flat Chl* ESA. The green EADS evolves in 33 ps to the magenta EADS, which is pure Chl*, that lives for about 2 ns. The difference with the 4 ns lifetime reported in [13] is attributed to the shorter time range used here. The normalized green DADS is most useful to interpret this 33 ps process. It consists of Chl* excited-state decay caused by annihilation (as evidenced by the decay of the Chl Q_y and Soret bleaches), and slowly decaying Per*. The latter possesses ESA that peaks just below 570 nm. The Per*–Chl energy transfer is very clear from the Chl Q_y features in the red and blue DADS, since decay of these features (with 0.6 and 2.3 ps) corresponds to rise of the Chl Q_y bleach. Note that on this time scale hardly any triplet is formed.

To resolve the many processes that occur in parallel, a target analysis is needed. From the above observations we propose the kinetic schemes depicted in Fig. 4. The peridinin–Chl scheme (left) resembles that used to analyse PCP before [6] and a similar light-harvesting complex [35], and also is in accordance with the scheme in [4]. All four Per* start in the S_2 state, and relax via hot S_1 to S_1 (three out of four pigments) and slow S_1 (one out of four pigments). Note that we do not use here a separate ICT state, which most probably is tightly connected to the S_1 state. In parallel to this evolution, all Per* states can transfer to Chl, and can decay to S_0, with different rates. To model Chl* annihilation we use two compartments (with equal SADS). An average annihilation rate is used, representing the hopping of Chl* until they encounter another Chl*, after which only a single Chl* is left. In the kinetic scheme, almost half of the Chl′* excitations are lost because the rate from Chl′* to the Chl ground-state (GS) is only a bit smaller than the rate from Chl′* to Chl*. In turn, Chl* decays to the GS in 2 ns.

The estimated rates are collated in the third column of Table 1, whereas Fig. 5 represents the estimated concentrations and SADS. The cyan SADS is identical to the black EADS and was discussed

[6] For interpretation to color in Figs. 1–4, 7–10, 12 and 13, the reader is referred to the web version of this article.

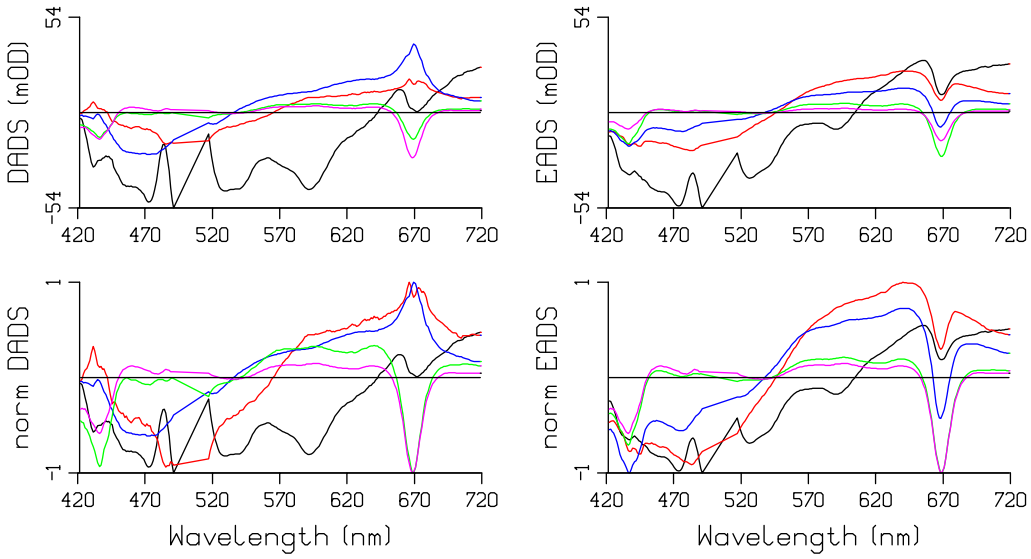

Fig. 3. Top row: DADS and EADS estimated from magic angle pump-probe data after 500 nm excitation. Bottom row shows normalized DADS and EADS. Key: 0.06 ps (black), 0.6 ps (red), 2.3 ps (blue), 33 ps (green), 1.9 ns (magenta). Note that (here and in Figs. 5 and 11) a straight line connects from 492 to 516 nm, because these data are missing. (For interpretation of color in this figure, the reader is referred to the web version of this article.)

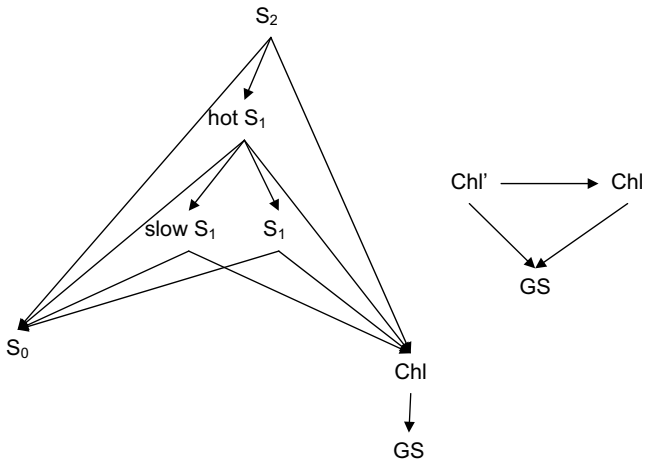

Fig. 4. Kinetic schemes used for the target analysis. Left, the channels of Per* excited-state evolution, Per* to Chl energy transfer and of Per* decay to its ground-state. Right, the scheme used to model Chl'* to Chl* annihilation. Further explanation is in text.

Table 1
Rate constants (in 1/ps) estimated from target analysis, using the kinetic schemes of Fig. 4.

From	To	Pump probe, RT	After prepump, RT	Pump probe, 77 K
S_2	Hot S_1	11	12	9.9
Hot S_1	S_1	0.6	0.6	0.6
Hot S_1	Slow S_1	0.2	0.2	0.2
S_1	Chl	0.40	0.32	0.40
Slow S_1	Chl	0.02	0.015	0.01
Chl	GS	0.0005	0.0005	0.001
S_2	Chl	4.1	2.3	5.1
Hot S_1	Chl	0.60	0.46	0.57
S_2	S_0	0.04	1.9	0.02
Hot S_1	S_0	0.04	0.2	0.02
S_1	S_0	0.04	0.13	0.02
Slow S_1	S_0	0.04	0.045	0.02
Chl′	Chl	0.019	0.015	0.057
Chl′	GS	0.013	0.017	0.032

Estimated relative error is 25%.

above. The red SADS represents hot S_1, showing broad ESA. The branching ratios from the excited Per states were adjusted to minimize the Chl Q_y features in their SADS. Thus the red, blue and green SADS are almost free from Chl Q_y features. The blue SADS represents S_1, showing a small blue shift (relative to the red SADS) of the isosbestic point. The green SADS, which represents slowly decaying S_1, shows less ESA above 600 nm. Its shape resembles more the S_1 SADS of Per as resolved from the equilibrium with ICT in methanol [23,26]. Thus its lack of ICT character might be the cause of its slow energy transfer to Chl. Other causes may be an unfavorable orientation (e.g. of the Per 612 and Per 622, cf. Fig. 1 and [8]), or less carotenoid backbone deformation. Note that from the target analysis we propose a lifetime of ≈16 ps for this slowly decaying S_1, which is largely due to a natural decay rate of 1/(25 ps), and to a smaller part due to energy transfer to Chl, with rate 1/(50 ps). The annihilation is adequately described by the 33 ps lifetime observed in the Chl* decay. With the excitation density used about 30% of the excitations are lost by annihilation. In reality the annihilation will be a multiexponential process, with a distribution of rates corresponding to different numbers of hops between Chl within and between trimers [13,36].

3.2. Testing the kinetic scheme with 475 nm excitation data

An independent experiment with 475 nm excitation and smaller time steps and shorter time range was successfully analysed with the same target kinetic scheme. Global analysis of these data yielded five lifetimes of ≈0.04 ps (black), 0.6 ps (red), 2.4 ps (blue), 20 ps (green). The difference between the 20 ps lifetime and the value of 33 ps found above, is attributed to the higher excitation density used here, resulting in somewhat faster annihilation and larger signals. The final lifetime was fixed at 2 ns (magenta). The estimated DADS and EADS are shown in Fig. S2. Although the first EADS shows differences, which are attributed to the larger imprecision with this short lifetime, in general the shapes are very similar to those of Fig. 3. In particular the green DADS consists of Chl* excited-state decay caused by annihilation (as evidenced by the decay of the Chl Q_y and Soret bleaches), and slowly decaying Per*, as evidenced by the decay of ESA around 560 nm and bleach around 480 nm. Target analysis using very similar parameters resulted in the SADS of Fig. S3. Again, the red, blue and green SADS

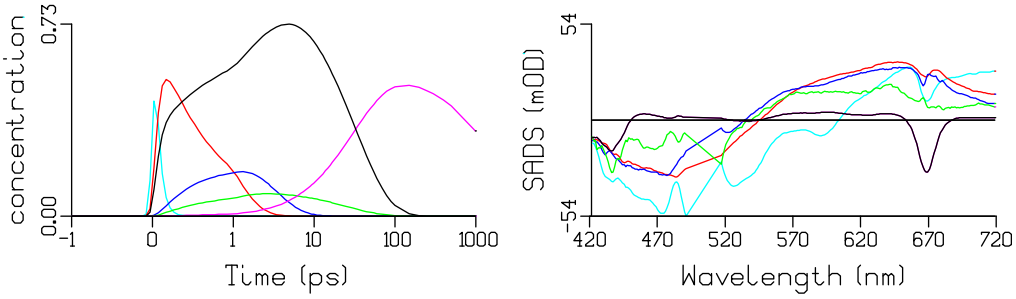

Fig. 5. Concentration profiles (left) and SADS (right) estimated from magic angle pump-probe data after 500 nm excitation using the kinetic schemes from Fig. 4. Key: S_2 (cyan), hot S_1 (red), S_1 (blue), slow S_1 (green), Chl (black), terminal Chl (magenta).

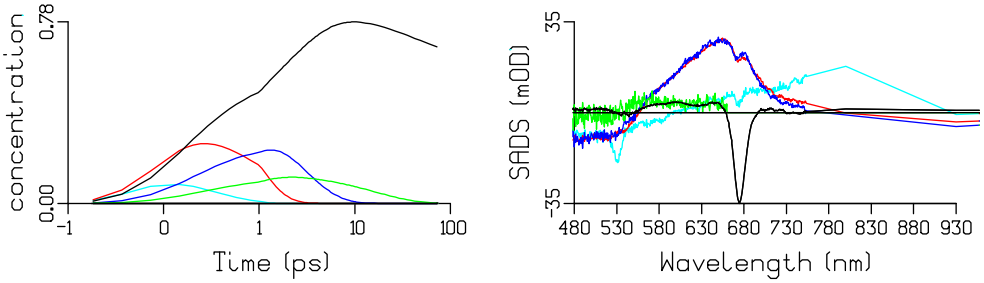

Fig. 6. Concentration profiles (left) and SADS estimated from magic angle pump-probe data after 535 nm excitation using the kinetic schemes from Fig. 4. Key: S_2 (cyan), hot S_1 (red), S_1 (blue), slow S_1 (green), Chl plus terminal Chl (black).

are almost free from Chl Q_y features. Since the SADS of the slowly decaying S_1 (green) is the smallest contribution to the data, hidden under the contributions of the other states, it is estimated less precisely than the others. Note that it is qualitatively very similar to that in Fig. 5, which corroborates our findings from the 500 nm excitation data.

3.3. Testing the kinetic scheme with visible and near IR data from [7].

The PCP model system and its components have been comprehensively studied in Sundström's laboratory in Lund. Here we apply our global and target analysis methods to measurements after 535 nm excitation in the visible and near IR as obtained by Zigmantas et al. [7], shown in Fig. S4. Most important is the 930 nm trace, which shows the decay of the stimulated emission from the Per S_1/ICT state, and rise towards the level of Chl ESA. Global analysis of these data yielded five lifetimes of ≈0.09 ps (black), 0.5 ps (red), 2.4 ps (blue), 20 ps (green). The final lifetime was fixed at 2 ns (magenta). The estimated DADS and EADS are shown in Fig. S5. Clearly both the red and blue EADS have negative amplitude at 930 nm. The green DADS consists of Chl* excited-state decay caused by annihilation (as evidenced by the decay of the Chl Q_y bleach), and slowly decaying Per*, as evidenced by the decay of ESA around 560 nm and bleach around 480 nm. But in contrast to the previous excitation wavelengths, the difference between the normalized green and magenta DADS is smaller. This indicates a smaller amount of slowly decaying S_1 in these 535 nm excitation measurements. Target analysis resulted in the SADS of Fig. 6. The green SADS has now become very small and noisy, and we assumed it to be zero above 650 nm. It does contain ESA around 560 nm and bleach around 480 nm. Again, the red and blue SADS are almost free from Chl Q_y features. Both show stimulated emission at 930 nm, indicating that both hot S_1 and S_1 are strongly coupled to the ICT state. Apparently, after 535 nm excitation only a small fraction (5–10%) of slowly decaying Per is present. In contrast, 490 nm excitation data from [7] are very comparable to the 500 and 475 nm data presented above. The estimated DADS and EADS in Fig. S6 show a clear Per* contribution in the normalized green DADS. Target analysis results of these 490 nm excitation data are depicted in Fig. 7. Again the green SADS shows a clear Per bleach, consistent with a 25% fraction of slowly decaying Per, and the ESA lacks ICT features. We propose that the slowly decaying

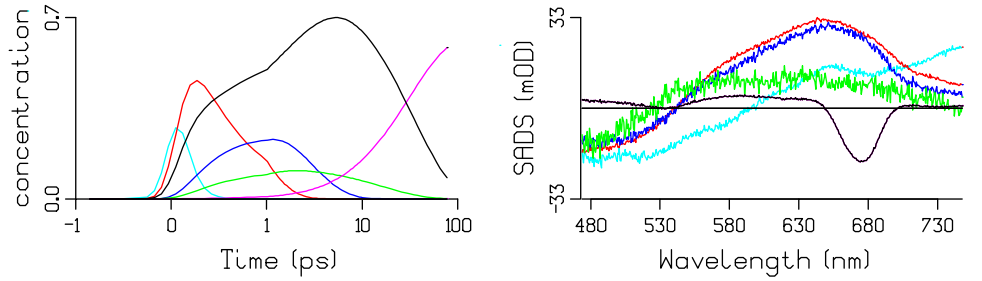

Fig. 7. Concentration profiles (left) and SADS estimated from magic angle pump-probe data after 490 nm excitation using the kinetic schemes from Fig. 4. Key: S_2 (cyan), hot S_1 (red), S_1 (blue), slow S_1 (green), Chl (black), terminal Chl (magenta). (For interpretation of color in this figure, the reader is referred to the web version of this article.)

Per is the most blue absorbing Per, which most likely corresponds to Per 612 and Per 622 [15,16] (colored blue in Fig. 1).

3.4. Testing the kinetic scheme with 77 K data

At lower temperature experiments with 500 and 520 nm excitation were performed, with a time range of 300 ps. Global analysis of the 520 nm excitation data yielded five lifetimes of 0.06 ps (black), 0.5 ps (red), 2.1 ps (blue), 14 ps (green), 0.9 ns (magenta). The final lifetime is not precise in view of the limited time range. The estimated DADS and EADS are shown in Figs. 8 and 9. The first EADS is less reliable, because the data suffered from a coherent artifact. Again the S_2 ESA is accompanied by a Chl Q_y bleach. Going from the second to the third to the fourth EADS the Chl Q_y bleach increases further, whereas the Per ESA decreases. The green DADS consists of Chl* excited-state decay caused by annihilation (as evidenced by the decay of the Chl Q_y bleach), and slowly decaying Per*, as evidenced by the decay of ESA from 570–700 nm (compare the normalized green and magenta DADS and EADS). However, also some spectral evolution is present in the Chl Q_y bleach, the minimum shifts by 1 nm from 664 to 665 nm. This shift is comparable to the 1 nm red shift measured at 10 K [16]. Thus the 14 ps time constant also encompasses a third process, transfer to the red most Chl pigment. This complication is dealt with in the target analysis by allowing the two Chl SADS to differ between 653 and 679 nm. The estimated rates are collated in the fifth column of Table 1, whereas Fig. 9 represents the estimated concentrations and SADS. Again the Per SADS (hot S_1, S_1 and slow S_1) are practically free from Chl Q_y features. In this way both Chl annihilation and spectral evolution have been described. Global analysis of the 500 nm excitation data was only slightly different, in that the relative amount of Chl annihilation was somewhat smaller, and the lifetime was now 21 ps, cf. Fig. S7. The S_1 lifetime at 77 K appears to be slightly shorter than that at room temperature, in agreement with the finding at 10 K [16]. We conclude that the kinetic scheme of Fig. 4 is adequate to describe also these 77 K data.

3.5. Prepumping Chl: additional Per*–Chl* interactions

To study Per*–Chl* interactions a multi-pump transient absorption experiment was performed, where a 500-nm pulse is used to excite peridinins while the chlorophylls in PCP have been pre-excited by a 400-nm pulse and are in their excited state [30]. Magic angle pump probe data measured after 500 nm excitation are depicted in Fig. 10 and Fig. S8. Black are the ordinary pump-probe traces already depicted in Fig. S1, blue is the prepump signal, which after 300 ps corresponds to an almost constant Chl* SADS. The red traces are from the 400-nm prepump followed after 300 ps by the 500-nm pump pulse. Note that at late times the black and red traces are almost identical, indicating that a lot of

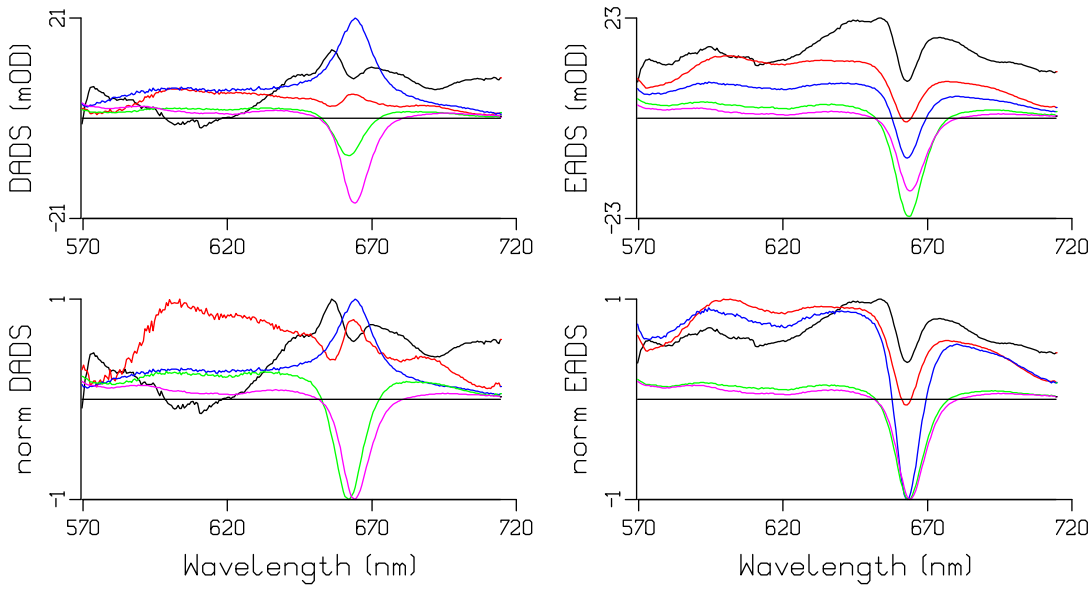

Fig. 8. Top row: DADS and EADS estimated from magic angle pump-probe data at 77 K after 520 nm excitation. Bottom row shows normalized DADS and EADS. Key: 0.06 ps (black), 0.5 ps (red), 2.1 ps (blue), 14 ps (green), 0.9 ns (magenta). (For interpretation of color in this figure, the reader is referred to the web version of this article.)

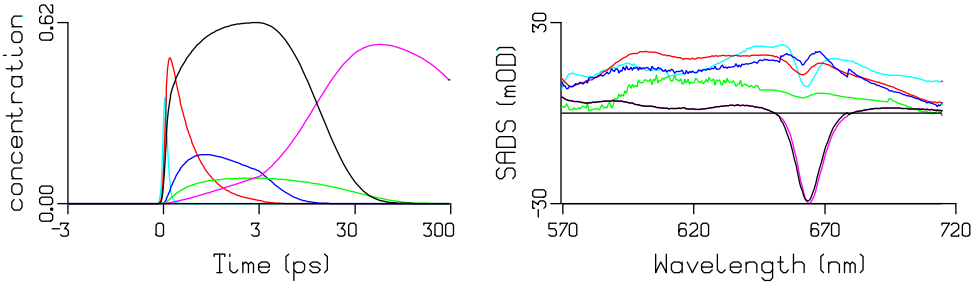

Fig. 9. Concentration profiles (left) and SADS (right) estimated from magic angle pump-probe data at 77 K after 520 nm excitation using the kinetic schemes from Fig. 4. Key: S_2 (cyan), hot S_1 (red), S_1 (blue), slow S_1 (green), Chl (black), terminal Chl (magenta). (For interpretation of color in this figure, the reader is referred to the web version of this article.)

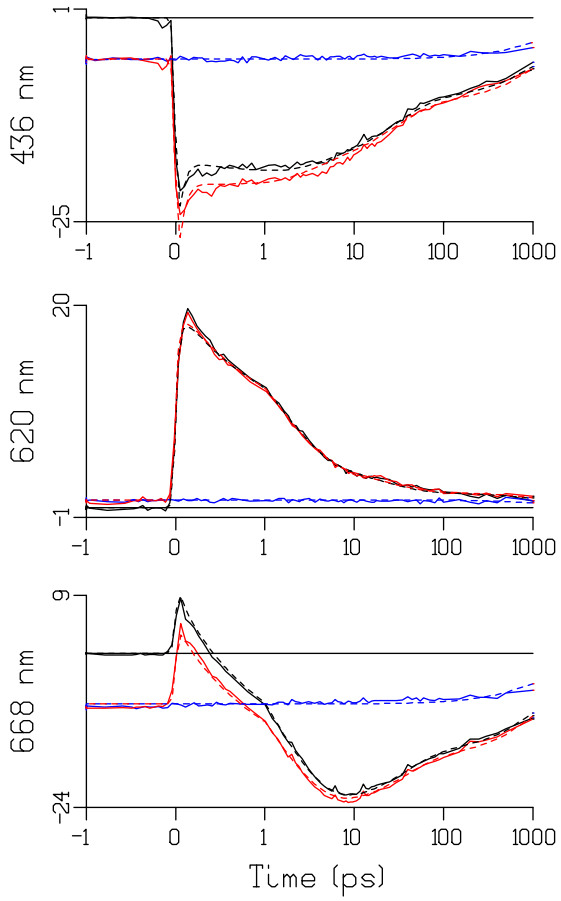

Fig. 10. Selected traces at three wavelengths (indicated as ordinate labels, vertical unit is mOD). Dashed lines indicate fit. The time axis is linear till 1 ps, and logarithmic thereafter. Black are the ordinary pump-probe traces, blue is the prepump signal, which corresponds to Chl*. The red traces are from the 400-nm prepump followed after 300 ps by the 500-nm pump pulse. (For interpretation of color in this figure, the reader is referred to the web version of this article.)

annihilation occurs. This is particularly well visible in the traces at 436 and 668 nm, which are representative of the Chl Soret and Q_y bleach. At early times the red signal is clearly more negative than the black signal, although due to Per* to Chl* annihilation the difference is already smaller than the difference with the blue prepump signal. At later times both Per* to Chl* and Chl* to Chl* annihilation diminish the difference between the black and red traces.

The above kinetic scheme was further tested in a simultaneous target analysis of these three experiments. It was shown in [30] that the rate of energy transfer from Per* to Chl does not depend on the acceptor being in the ground or excited state. If Chl is already in the excited state, then after Per* to Chl* energy transfer a single Chl* remains. Thus to describe the Per*–Chl* annihilation only the decay rates of Per* states to S_0 had to be modified. The estimated rates are collated in the fourth column of Table 1, whereas Fig. 11B represents the estimated SADS. The SADS are very similar to those from Fig. 5B, and the estimated rates appear realistic. Likewise, the prepumped 475 nm excitation data were successfully described by the concentrations and SADS depicted in Fig. S9. We conclude that the kinetic scheme of Fig. 4 is also adequate to describe these complicated annihilation data.

3.6. Per–Chl* interactions: excitation of chlorophyll-a at 670 nm

We used 670 nm pulses to directly excite the chlorophylls in PCP to their Q_y state and probe the resulting dynamics. Fig. S11 contains traces measured for the three different relative polarizations. Global analysis of the magic angle data (black in Fig. S11) yielded the EADS and DADS shown in Fig. S10. The first few hundred femtoseconds which are dominated by coherent artifact and Raman scattering have been omitted from the data analysis. Thereafter the data are well described by two lifetimes of about 12 ps and 2.3 ns. There is hardly any spectral evolution, and we interpret the 12 ps lifetime as Chl–Chl annihilation. Thus the first and second EADS are considered almost identical.

The EADS contains the contribution of the Chl Q_y bleach around 670 nm. A weak ESA covers the entire spectral region, presumably originating from the Q_y of chlorophyll. Notably, around 540 nm the spectra contain a dip, superimposed on the Chl ESA. This bleach-like feature was observed also before [6,18], and in the above described Chl SADS. Ascribing it to a transition is not straightforward as the Chl Q_x transition has been suggested to lie around 600 nm [12]. We attribute the 540-nm feature to a peridinin molecule, which absorbs in that region and may respond to a neighboring Chl*, as illustrated for the carotenoids in bacterial [37,38] and plant LH complexes [39]. To further investigate this feature polarized pump-probe was used.

Traces at three representative wavelengths are shown in Fig. 12. Comparing the three different polarizations qualitatively, the Chl Q_y (667 nm) has a high positive anisotropy, which is what would be expected, at least at early times, before Chl → Chl transfer takes place. The anisotropy of the ESA (597 nm) appears to be lower than that of the Q_y, which is to be expected as the corresponding transition dipole moment(s) are not necessarily parallel to that of Q_y. Nevertheless, the ESA anisotropy is still positive. Judged from the traces at 542 nm in Fig. 12, and between 527 and 557 nm in Fig. S10, the anisotropy of the 540-nm feature is certainly positive and larger than that of the ESA. This consolidates that this feature is not related to the Q_x state, which should exhibit a negative anisotropy because its dipole moment is at an angle of 90° from that of Q_y.

For a target analysis of these anisotropy data we will need three "species", which decay identically at magic angle (with lifetimes of 12 ps and 2.3 ns). The Chl Q_y bleach contributes only above

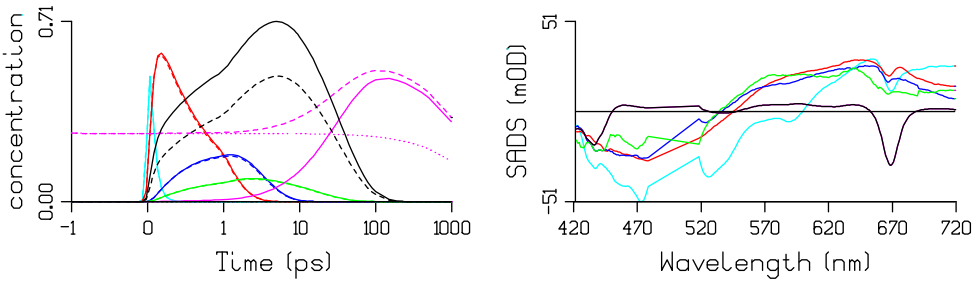

Fig. 11. Concentration profiles (left) and SADS estimated from magic angle data after 500 nm excitation using the kinetic schemes from Fig. 4. The dotted concentrations are from the prepump experiment, the solid lines are from the normal pump-probe experiment, and the dashed lines correspond to the combined prepump-pump-probe experiment. Key: S_2 (cyan), hot S_1 (red), S_1 (blue), slow S_1 (green), Chl (black), terminal Chl (magenta).

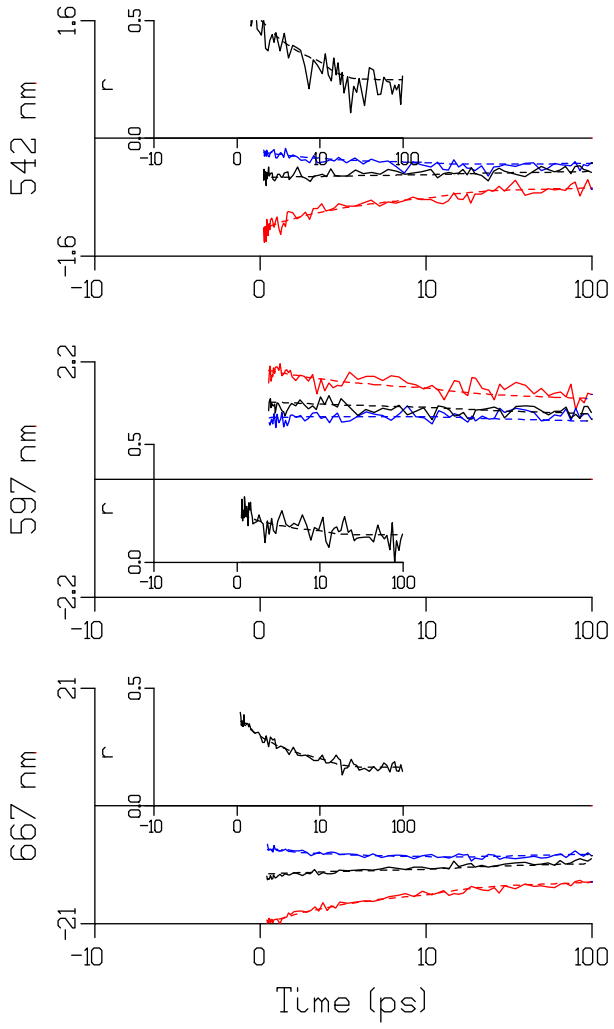

Fig. 12. Selected traces at wavelengths (indicated as ordinate labels, vertical unit is mOD) from polarized pump-probe data after 670 nm excitation. Inset depicts calculated anisotropy. Dashed lines indicate fit. The time axis is linear till 10 ps, and logarithmic thereafter. The black, red, and blue color correspond to, respectively, magic angle, parallel and perpendicular orientation. (For interpretation of color in this figure, the reader is referred to the web version of this article.)

650 nm. The Chl ESA contributes everywhere, and will have a different anisotropy. Finally, the peridinin bleach feature is assumed to contribute between 519 and 573 nm. Furthermore, we assumed a Chl Q_y bleach anisotropy after 100 ps of 0.16, based upon [13]. The estimated SAS are depicted in Fig. 13. The shapes of the bleach of Chl Q_y and the partial bleach of peridinin appear realistic. The

Table 2
Anisotropy parameters estimated from target analysis of 670 nm excitation data. Estimated relative error is 10%. Estimated magic angle lifetimes 12 ps and 2.3 ns, and anisotropy decay time 6 ps.

	r_0	r_∞
Chl Q_y	0.36	0.16 (fixed)
Chl ESA	0.21	0.12
Per bleach	0.36	0.16 (fixed)

Chl ESA shows some wiggles in the regions of overlap with these bleaches. The estimated anisotropy parameters are collated in Table 2. A value of 6 ps is found for the anisotropy decay time, which corresponds well to previous values found for intra-monomer energy transfer between chlorophylls [13].

From this target analysis the anisotropy of the partial bleach of peridinin appears not to differ significantly from that of the Chl Q_y bleach. In the crystal structure only peridinins 614 and 624 (colored orange in Fig. 1) have an S_2 transition which is parallel to the Chl Q_y transition. This was confirmed by structure based calculations [31], which show that contributions from all other three peridinins would have an initial anisotropy of 0.06 or less in these measurements. The fact that peridinin 614 and 624 interact most strongly with Chl makes sense, since their center-to-center distance to Chl is 7 Å, while the other peridinins are at 11 Å [3]. This way, a specific spectral feature was assigned to peridinin 614 and 624 from the PCP structure. The specific involvement of Per 614/624 in chlorophyll triplet quenching was demonstrated by time resolved EPR in [40].

4. Conclusion

Target analysis using the kinetic scheme from Fig. 4 successfully described the dynamics and interactions in PCP. Annihilation between Per* and Chl*, or between two Chl*, can be well approximated by an exponential decay. We found no evidence in PCP that the peridinin S_1 and the ICT states are separate entities, as in peridinin in methanol [23,26]. However, we established that the long lived peridinin in PCP more resembles the S_1 state, and shows hardly any ICT related spectral features. Based upon the smaller contribution with 535 nm excitation, we assign it to the most blue absorbing Per, which most likely corresponds to Per 612 and Per 622 [15,16]. At 77 K, the dynamics are very similar to those at room temperature. Spectral equilibration takes place in about 15 ps between the two Chl, whose absorbance maxima are 1 nm apart. After 670 nm excitation, the anisotropy decays in 6 ps. Most likely, the peridinins 614 and 624 exhibit a strong Per–Chl interaction, which results in a partial bleach around 540 nm when Chl is excited.

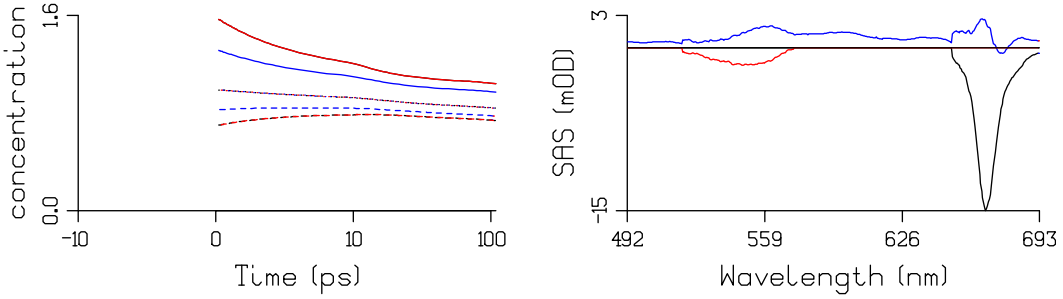

Fig. 13. Concentration profiles (left) and SAS (right) estimated from polarized pump-probe data after 670 nm excitation. The dotted, solid, and dashed concentrations correspond to, respectively, magic angle, parallel and perpendicular orientation. Key: Per bleach (red), Chl ESA (blue), Chl bleach (black). Note that the red and black concentrations are identical, and that all magic angle concentrations are identical. (For interpretation of color in this figure, the reader is referred to the web version of this article.)

Acknowledgements

This research was supported by The Netherlands Organization for Scientific Research (NWO) via the Dutch Foundation for Earth and Life Sciences (ALW). M.V. received financial support from the Stichting voor Fundamenteel Onderzoek der Materie, Netherlands (FOM). D.S.L. is grateful to the Human Frontier Science Program Organization for providing financial support with a long-term fellowship.

Appendix A. Supplementary material

Supplementary data associated with this article can be found, in the online version, at doi:10.1016/j.chemphys.2008.10.005.

References

[1] R.G. Hiller, H.A. Frank, A.J. Young, G. Britton, R.J. Cogdell (Eds.), Photochemistry of Carotenoids, Kluwer Academic Publishers, Dordrecht, the Netherlands, 1999, p. 81.
[2] F.P. Sharples, P.M. Wrench, K.L. Ou, R.G. Hiller, Biochim. Biophys. Acta-Bioener. 1276 (1996) 117.
[3] E. Hofmann, P.M. Wrench, F.P. Sharples, R.G. Hiller, W. Welte, K. Diederichs, Science 272 (1996) 1788.
[4] T. Polívka, R.G. Hiller, H.A. Frank, Arch. Biochem. Biophys. 458 (2007) 111.
[5] J.A. Bautista, R.G. Hiller, F.P. Sharples, D. Gosztola, M. Wasielewski, H.A. Frank, J. Phys. Chem. A 103 (1999) 2267.
[6] B.P. Krueger, S.S. Lampoura, I.H.M. van Stokkum, E. Papagiannakis, J.M. Salverda, C.C. Gradinaru, D. Rutkauskas, R.G. Hiller, R. van Grondelle, Biophys. J. 80 (2001) 2843.
[7] D. Zigmantas, R.G. Hiller, V. Sundström, T. Polívka, P. Natl. Acad. Sci. USA 99 (2002) 16760.
[8] A. Damjanovic, T. Ritz, K. Schulten, Biophys. J. 79 (2000) 1695.
[9] J. Zimmermann, P.A. Linden, H.M. Vaswani, R.G. Hiller, G.R. Fleming, J. Phys. Chem. B 106 (2002) 9418.
[10] S. Akimoto, S. Takaichi, T. Ogata, Y. Nishimura, I. Yamazaki, M. Mimuro, Chem. Phys. Lett. 260 (1996) 147.
[11] R.P. Ilagan, S. Shima, A. Melkozernov, S. Lin, R.E. Blankenship, F.P. Sharples, R.G. Hiller, R.R. Birge, H.A. Frank, Biochemistry 43 (2004) 1478.
[12] F.J. Kleima, M. Wendling, E. Hofmann, E.J.G. Peterman, R. van Grondelle, H. van Amerongen, Biochemistry 39 (2000) 5184.
[13] F.J. Kleima, E. Hofmann, B. Gobets, I.H.M. van Stokkum, R. van Grondelle, K. Diederichs, H. van Amerongen, Biophys. J. 78 (2000) 344.
[14] P.A. Linden, J. Zimmermann, T. Brixner, N.E. Holt, H.M. Vaswani, R.G. Hiller, G.R. Fleming, J. Phys. Chem. B 108 (2004) 10340.
[15] S. Shima, R.P. Ilagan, N. Gillespie, B.J. Sommer, R.G. Hiller, F.P. Sharples, H.A. Frank, R.R. Birge, J. Phys. Chem. A 107 (2003) 8052.
[16] R.P. Ilagan, J.F. Koscielecki, R.G. Hiller, F.P. Sharples, G.N. Gibson, R.R. Birge, H.A. Frank, Biochemistry 45 (2006) 14052.
[17] T. Polívka, T. Pascher, R.G. Hiller, Biophys. J. 94 (2008) 3198.
[18] T. Polívka, T. Pascher, V. Sundström, R.G. Hiller, Photosynth. Res. 86 (2005) 217.
[19] S. Mackowski, S. Wormke, T.H.P. Brotosudarmo, C. Jung, R.G. Hiller, H. Scheer, C. Brauchle, Biophys. J. 93 (2007) 3249.
[20] J.A. Bautista, R.E. Connors, B.B. Raju, R.G. Hiller, F.P. Sharples, D. Gosztola, M.R. Wasielewski, H.A. Frank, J. Phys. Chem. B 103 (1999) 8751.
[21] D. Zigmantas, T. Polívka, R.G. Hiller, A. Yartsev, V. Sundström, J. Phys. Chem. A 105 (2001) 10296.
[22] D. Zigmantas, R.G. Hiller, A. Yartsev, V. Sundström, T. Polívka, J. Phys. Chem. B 107 (2003) 5339.
[23] E. Papagiannakis, D.S. Larsen, I.H.M. van Stokkum, M. Vengris, R. Hiller, R. van Grondelle, Biochemistry 43 (2004) 15303.
[24] H.M. Vaswani, C.P. Hsu, M. Head-Gordon, G.R. Fleming, J. Phys. Chem. B 107 (2003) 7940.
[25] L. Premvardhan, E. Papagiannakis, R.G. Hiller, R. van Grondelle, J. Phys. Chem. B 109 (2005) 15589.
[26] E. Papagiannakis, M. Vengris, D.S. Larsen, I.H.M. vanStokkum, R.G. Hiller, R. vanGrondelle, J. Phys. Chem. B 110 (2006) 512.
(27) T. Polívka, V. Sundström, Chem. Rev. 104 (2004) 2021.
[28] C.C. Gradinaru, I.H.M. van Stokkum, A.A. Pascal, R. van Grondelle, H. van Amerongen, J. Phys. Chem. B 104 (2000) 9330.
[29] D.S. Larsen, M. Vengris, I.H.M. van Stokkum, M.A. van der Horst, R.A. Cordfunke, K.J. Hellingwerf, R. van Grondelle, Chem. Phys. Lett. 369 (2003) 563.
[30] M. Vengris, Biological Photoreactions Explored by Multi-Pulse Ultrafast Spectroscopy, Ph.D. Thesis, Vrije Universiteit, Amsterdam, 2005.
[31] J.M. Salverda, Interacting Pigments in Light-Harvesting Complexes Studied with Nonlinear Spectroscopy, Ph.D. Thesis, Vrije Universiteit, Amsterdam, 2003.
[32] S.S. Lampoura, Dynamics in Biological Samples and J-Aggregates Explored by Linear and Non-linear Optical Spectroscopy, Ph.D. Thesis, Vrije Universiteit, Amsterdam, 2001.
[33] I.H.M. van Stokkum, D.S. Larsen, R. van Grondelle, Biochim. Biophys. Acta 1657 (2004) 82.
[34] I.H.M. van Stokkum, D.S. Larsen, R. van Grondelle, Biochim. Biophys. Acta 1658 (2004) 262.
[35] T. Polívka, I.H.M. van Stokkum, D. Zigmantas, R. van Grondelle, V. Sundström, R.G. Hiller, Biochemistry 45 (2006) 8516.
[36] H. van Amerongen, L. Valkunas, R. van Grondelle, Photosynthetic Excitons, World Scientific Publishing, Singapore, 2000.
[37] J.L. Herek, T. Polívka, T. Pullerits, G.J.S. Fowler, C.N. Hunter, V. Sundström, Biochemistry 37 (1998) 7057.
[38] J.L. Herek, M. Wendling, Z. He, T. Polívka, G. Garcia-Asua, R.J. Cogdell, C.N. Hunter, R. van Grondelle, V. Sundström, T. Pullerits, J. Phys. Chem. B 108 (2004) 10398.
[39] C.C. Gradinaru, R. van Grondelle, H. van Amerongen, J. Phys. Chem. B 107 (2003) 3938.
[40] M. Di Valentin, S. Ceola, E. Salvadori, G. Agostini, D. Carbonera, Biochim. Biophys. Acta Bioener. 1777 (2008) 186.